COHERENT OPTICAL DATA PROCESSING: A STATUS REPORT

DAVID CASASENT

Carnegie-Mellon University, Pittsburgh, PA 15213
EASCON, Washington, D.C.

ABSTRACT

The operations possible in a coherent optical computer are briefly reviewed and several applications of this novel class of processor are included. Emphasis is given to signal processing operations and new space variant optical processor architectures.

1. INTRODUCTION

The operations possible in a coherent optical computer are well known [1,2] and are thus only briefly reviewed in Section 2. The advantages of optical computing include: parallel processing, high space bandwidth, and high throughput. The high space or time bandwidth of an optical system is vividly demonstrated in the folded spectrum analyzer presented in Section 3. To demonstrate the parallel processing of these systems and their high throughput, we include several image processing and signal processing examples in Sections 6 and 7. To realize the high throughput of this processor, real time and reusable spatial light modulators are essential. The status of the leading candidate 2-D transducers are briefly summarized in Section 4. One of the shortcomings of an optical processor is its lack of flexibility and the limited number of operations possible in an optical processor. One way of extending the flexibility of these optical processors is to combine an optical and digital system into a hybrid processor. We briefly review current work on such systems in Section 5. Another recent approach to optical processing whereby the repertoire of operations achievable can be increased and many practical problems overcome, is the optical space variant processor. The highlights of recent research in this area are included in Section 8. The multitude of topics and wealth of results to be discussed preclude extensive description of any one application; these details are available in the references noted.

2. OPTICAL COMPUTING

The schematic diagram of the optical data processor which we will use to describe the operation possible in an optical computer is shown in Figure 1. Plane P_1 is the input plane in which a transparent version of the input data (signal or image) to be processed is placed. Because we consider only coherent optical computers herein, the spatial amplitude transmittance of plane P_1 or the input 2-D data are assumed to be $g(x_1,y_1)$. The light distribution incident on plane P_2 (the back focal plane of lens L_1) is the 2-D Fourier transform of g or

$$G(u,v) = \iint g(x_1,y_1) \exp[-j2\pi(x_1u + y_1v)]dx_1dy_1. \quad (1)$$

Capital letters (e.g., G) are used to denote the Fourier transforms of the corresponding lower case variables (e.g., g). The coordinates (u,v) of plane P_2 are spatial frequencies which are related to the distance coordinates (x_2,y_2) of plane P_2 by $(x_2,y_2) = (u,v)\lambda f_1$, where λ is the wavelength of the laser light used and f_1 is the focal length of the Fourier transform lens L_1.

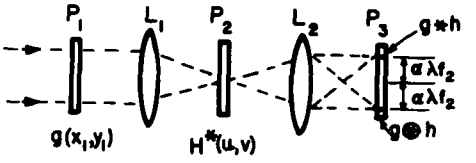

Fig. 1 Schematic representation of a frequency plane correlator.

In the output plane P_3, lens L_2 forms the Fourier transform of the light distribution G(u,v) in its front focal plane P_2, and in plane P_3 we find an image of $g(x_1,y_1)$. By placing simple opaque spots in plane P_2, various spatial frequencies present in the input image can be removed. With an opaque spot in the central or dc frequency region of plane P_2, the output image will be a high-pass filtered or differentiated version of the input image. This is known as spatial filtering. With more complex spatial filters at plane P_2 (e.g., those that spatially alter both the phase and amplitude of the function), images can be restored and enhanced, blurred or defocused images can be restored, etc.

With the transmittance of plane P_2 described by the Fourier transform H(u,v) of h(x,y) and

with g(x,y) placed at plane P_1, the light distribution incident on plane P_2 is G(u,v) and the light distribution transmitted through plane P_2 is G·H. Lens L_2 forms the transform of this product of two transforms and at plane P_3 the output pattern is the convolution g*h of g and h. This is the basic operation used in image enhancement and restoration and is equivalent to altering the impulse response or point spread function of the system.

If we can make the amplitude transmittance of plane P_2 proportional to the complex conjugate H^* of the Fourier transform H of a reference function h (we discuss how this is possible below), then with g(x,y) at plane P_1, the light distribution transmitted through plane P_2 is GH^* and in plane P_3 we obtain the correlation $g \circledast h$ of the input and reference function. This is the basic operation used in pattern recognition and in processing coded waveforms and signals in radar, sonar, etc. The resultant system of Figure 1 is then known as a frequency plane correlator and the pattern H^* at plane P_2 as a matched spatial filter.

To record this H^* pattern at plane P_2, we use the principle of holography. At plane P_1, we place a transparency with amplitude transmittance h(x,y), i.e., the reference function. Its Fourier transform H(u,v) produced by lens L_1 is incident on plane P_2. At plane P_2, we record the interference of H(u,v) and an off-axis plane wave reference beam $A \exp(-j2\pi\alpha x_2)$ (where A is the uniform amplitude of the plane wave and $\alpha = (\sin\theta)/\lambda$ where θ is the off-axis angle between the reference beam and reference function. The recording material at plane P_2 is intensity sensitive and the subsequent transmittance of plane P_2 is

$$\begin{aligned} t(x_2,y_2) &= |H + A\exp(j2\pi\alpha x_2)|^2 \\ &= |H|^2 + |A|^2 + HA\exp(j2\pi\alpha x_2) \\ &\quad + H^*A\exp(-j2\pi\alpha x_2). \end{aligned} \tag{2}$$

The last term in Eq. (2) is proportional to the desired H^* term and can be separated from the other terms in Eq. (2) by proper choice of the angle θ (which is encoded in α).

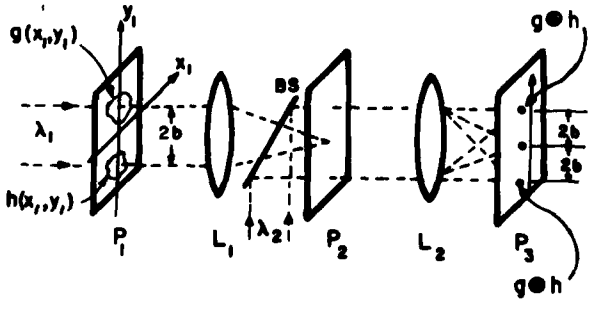

Fig. 2 Schematic representation of a reflex readout joint transform correlator.

An alternate optical correlator topology is shown in Figure 2. In this schematic, the two functions g and h to be correlated are placed side-by-side in plane P_2 separated by a center-to-center distance 2b. The transmittance of P_1 in 1-D is described by

$$U(y_1) = g(y_1-b) + (y_1+b). \tag{3}$$

At plane P_2 we record:

$$\begin{aligned} t(v) &= |G(v)\exp(-j2\pi vb) + H(v)\exp(j2\pi vb)|^2 \\ &= |G|^2 + |H|^2 + GH^*\exp(-j4\pi vb) \\ &\quad + G^*H\exp(+j4\pi vb). \end{aligned} \tag{4}$$

Lens L_2 forms the Fourier transform of this pattern at plane P_3, where we find:

$$\begin{aligned} U(x_3,y_3) &= g*g + h*h \text{ at } (x_3,y_3) = (0,0) \\ &\quad + g \circledast h \text{ at } (x_3,y_3) = (0,2b) \\ &\quad + h \circledast g \text{ at } (x_3,y_3) = (0,-2b) \end{aligned} \tag{5}$$

where equal focal lengths $f_1 = f_2$ have been assumed for L_1 and L_2.

Many versions of these two systems exist. In Figure 2, we showed the recording of the pattern at plane P_2 with one wavelength of light and the reading of this pattern with a different wavelength of light in transmission from beam-splitter BS. The plane P_2 material is often read out in reflection in which case the beam splitter is placed to the right of plane P_2. In another version of either system, we can record N signals g_n on N lines at plane P_1 and replace lens L_1 with a cylindrical/spherical lens pair. The pattern at plane P_2 then consists of N Fourier transforms G_n of the N input signals g_n on N lines. With a cylindrical/spherical lens pair for lens L_2 and the same N reference 1-D signal H^* on N lines at plane P_2, the output pattern at plane P_3 consists of N correlations $g_n \circledast h$ on N separate lines. This multichannel 1-D correlator can be modified for use in radar processing by use of a spherical lens for L_2. The correlation of the N input signals g_n with the reference signal h (now a coded reference radar waveform) still occurs and we realize pulse compression. The vertical transform down the N lines in P_2 produces Doppler processing (in a pulse burst radar) or provides target azimuth data (in a phased array radar). Examples of these and other versions of these basic correlators are included in Sections 6, 7, and 8.

3. FOLDED SPECTRUM OPTICAL SIGNAL PROCESSING [3,4]

As one example of optical signal processing that vividly demonstrates the large time or space bandwidth product of an optical processor, we consider a long 1-D signal s(t) of T sec duration raster recorded on n lines in plane P_1 of Figure 1 with p points per line at a line scan rate

$f_H = 1/T_H$ (where T_H is the horizontal line scan time). The 2-D Fourier transform of this pattern is recorded at plane P_2 (lens L_2 and plane P_3 of Figure 1 are not used in this application). This pattern is a folded spectrum consisting of p horizontal coarse frequency loci with n fine frequency points per line. Frequencies from 0 to f_H present in the input signal appear on the first line in plane P_2 as spots of light, frequencies from f_H to $2f_H$ on line 2, etc. up to a maximum frequency pf_H on line p.

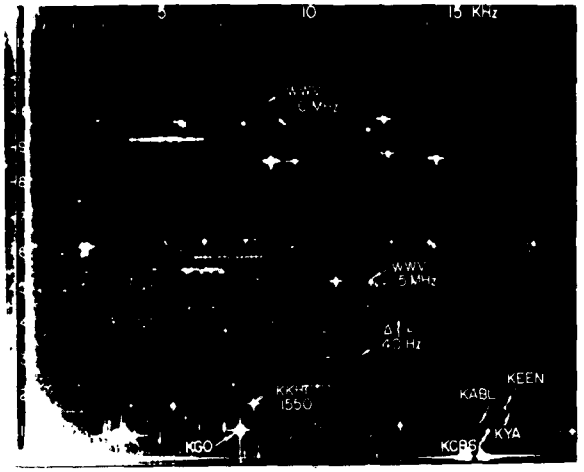

Fig. 3 Folded spectrum output of the RF spectrum with 12 MHz bandwidth and 40 Hz frequency resolution (Courtesy Ampex Corp.).

In Figure 3, a folded spectrum output pattern of a 25 msec record of the RF spectrum is shown. For this case, 750 raster lines were recorded with 400 cycles/line. The folded spectrum pattern has a 12 MHz bandwidth, with 400 coarse norizontal frequency loci and 750 fine frequencies per line for a 40 Hz fine frequency resolution in a 12 MHz signal bandwidth. Many specific stations and frequencies are noted on the figure.

4. REAL-TIME REUSABLE SPATIAL LIGHT MODULATORS [5,6]

Producing transparencies of the input g(x,y) data and the required filter functions such as $H^*(u,v)$ at rates comparable with the throughput of an optical processor requires real-time and reusable spatial light modulators (SLMs) in place of photographic film at planes P_1 and P_2. The desired data can be recorded on these devices by modulating the beam current of an off-axis electron gun with the input signal in sync with the scan of the electron beam. These electron beam addressed devices are useful for recording the input data at plane P_1. The major candidate electron beam addressed SLMs and their specifications are listed in the top of Table 1. TV frame rates (33 msec) are the generally accepted norm for real time although many of these devices can be operated faster.

The matched filter or reference filter function recorded at plane P_2 is usually easiest formed using an optically addressed SLM. These devices generally consist of a photo-conductor and electro-optic crystal sandwiched between two transparent electrodes with a dielectric mirror layer inside the structure. They are generally read-out in reflection as noted in the discussion of Figure 2. The leading candidate optically addressed SLMs for use at plane P_2 and their specifications are listed in the bottom of Table 1.

5. HYDRID OPTICAL/DIGITAL PROCESSORS [7,8]

To realize the high speed and parallel processing advantages of an optical processor as well as the flexibility, programability, and control features of a digital processor, a hybrid optical/digital system has been considered. The general schematic of one such system is shown in Figure 4. The top portion of the diagram is an optical correlator with real-time input and filter plane SLMs. The Fourier transform and correlation planes of this system are interfaced to the digital section of the hybrid processor through separate detector arrays. The interface digitizes the contents of these planes into an nxm cellular array. One function of the rest of the digital system is to extract the location and amplitude of the "important" peaks of light in these planes and of course to determine which are the important peaks of light.

These operations are achieved by thresholding, peak detection, area calculations, interframe operations (addition, subtraction, etc.). These are achieved by software or hardware and a repertoire of standard image processing operations in Basic. A PDP-11/15 computer with 64K of core and an RT-11 operating system are the master system. An array of 32 microprocessors and a 4K 250 nsec buffer memory are used to limit data flow to the PDP-11. The digital preprocessor consists of a floppy disc system, a magnetic tape unit, and a 2 Mbit (512 x 512 x 8 bit) store whose total contents can be randomly dumped in 30 msec. As the control lines in Figure 4 indicate, the digital system is used to control the data flow, the contents of the SLMs at planes P_1 and P_2, and the operation (write/read/or erase mode selection) of the real-time SLMs. The digital system also controls the output data displays (TV, x-y CRT, isometric display, histogram data, etc.). Examples of several of these hybrid system operations are included in Sections 6 and 7.

Table 1. Candidate real-time and reusable spatial light modulators and their specifications. The first three are electron-beam addressed, the last three are optically addressed.

DEVICE	RESOLUTION	STORAGE	CYCLE TIME	BANDWIDTH
E-Beam DKDP	1000 x 1000	1 hr.	33 msec	20 MHz
TOPR	1800 x 1800	days	2 sec	70 MHz
Dielectric	500 x 500	30 msec	33 msec	10 MHz
				SENSITIVITY
Photo DKDP	760 x 500	2 hrs.	1 msec	10 ergs/cm^2
Prom	250 x 250	10 min	1 msec	5000 ergs/cm^2
Liquid Crystal	650 x 650	15 msec	33 msec	5 ergs/cm^2

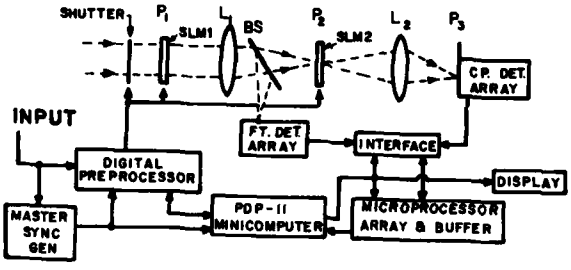

Fig. 4 Schematic diagrams of a hybrid optical/digital processor.

6. OPTICAL SIGNAL PROCESSING [9]

The highlights of several examples of optical signal processing follow. Limited space permits only brief remarks on each, an example of the output data, and reference to the original work for more details. In all applications, control of the input data format is important and the location of the output peaks of light are proportional to the target's azimuth, elevation, range, Doppler, etc. depending on the radar used. The hybrid optical processor of Figure 4 is used for all applications and the electron-beam DKDP light valve in the input plane P_1. Thus all applications that follow were performed in real-time at cycle times of 30 frames/sec.

6.1 Phased Array Radar Optical Signal Processing [10]

The electrical signal excitations applied to the elements of a phased array and the resultant

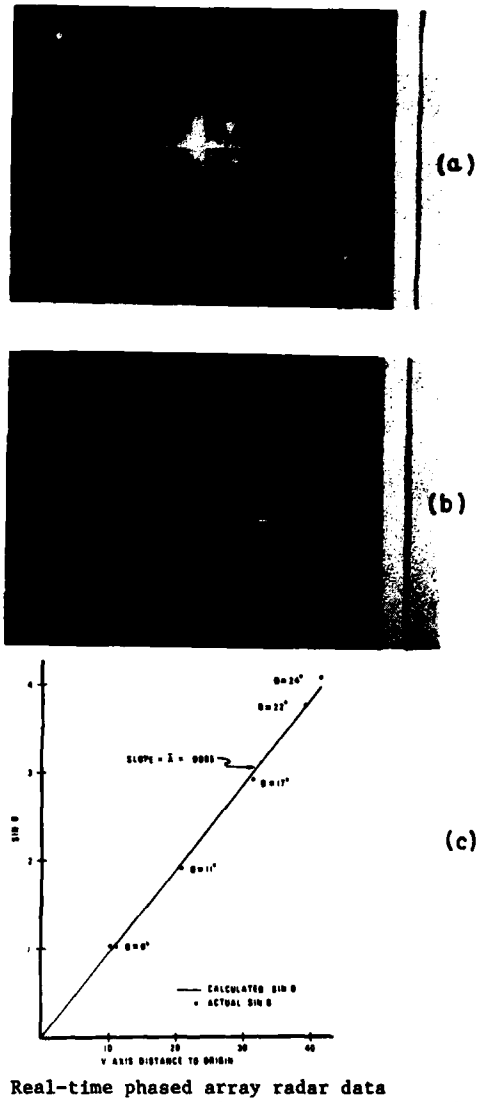

Fig. 5 Real-time phased array radar data processing using electron beam DKDP. The horizontal coordinates of the off-axis spots are proportional to the target's azimuth angle. (a) Optical output pattern; (b) Digitized version of (a); (c) Calculated vs. measured values of azimuth. [10]

radiation pattern are Fourier transform pairs. The dual relationship states that the received signal pattern and the location of the radiating object are also Fourier transform pairs. For simplicity, consider a linear phased array of N elements. If the time history of the received signals from the N elements of the array are recorded on N lines on the electron-beam KDKP at plane P_1, the 2-D Fourier transform of this input pattern (appearing at plane P_2) consists of a central dc term and two off-axis peaks of light. A typical output Fourier transform pattern is shown in Figure 5a. The horizontal coordinates of the two off-axis peaks of light are proportional to the target's azimuth angle and thus represent the desired output plane data.

After digital processing to remove the central dc term and determine the coordinates of the off-axis terms in Figure 5a, the simpler display of Figure 5b results. Extensive phased array data was processed and in all cases excellent agreement with the predicted values obtained (see Figure 5c). The optical processor easily accommodates multiple targets. In this case, multiple output peaks of light result; an example of this for pulsed Doppler radar follows. Planar phased array radar data has been processed by similar methods; in this case, the coordinates of the output off-axis peak of light are proportional to the target's elevation and azimuth angles.

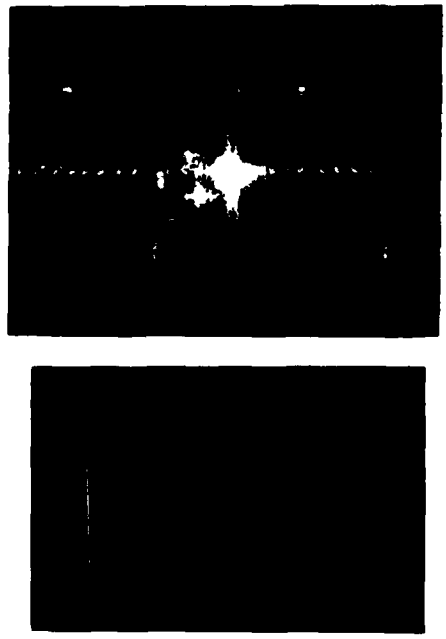

(a)

(b)

Fig. 6 Real-time pulsed Doppler radar data optical processing using electron beam DKDP. The horizontal coordinates of the off-axis spots are proportional to the target's Doppler velocity. (a) Optical output pattern; (b) Digitized version of (a). [11]

6.2 Pulsed Radar Optical Signal Processing [11]

To optically process pulsed Doppler or FM stepped radar data, N received signals are written on N lines on the electron beam DKDP device at plane P_1 (with a horizontal scan rate equal to the radar's prf) and the 2-D Fourier transform of this input pattern viewed at plane P_2. The output pattern is similar to that of Figure 5a except that the horizontal coordinates of the off-axis peaks of light are now proportional to the target's fine velocity (Doppler radar) or fine range (FM stepped radar). In Figure 6a, the output plane pattern for real pulsed Doppler radar data is shown. The two pairs of off-axis peaks of light correspond to two aircraft crossing in the same range bin at two different Doppler velocities. This pattern, after digital processing, is shown in Figure 6b from which the velocities of the two targets have easily been found.

6.3 Range/Doppler or Azimuth/Range Optical Signal Processing [12]

To extend this optical signal processing technique for use with coded radar waveforms, the full system of Figure 4 is used with a cylindrical/spherical lens pair for L_1. N identical reference signals of the coded radar waveform are recorded on N lines at P_1 and a multi-channel 1-D matched spatial filter of the coded reference waveform recorded at plane P_2. N pulse-burst radar returns or the received signals from N elements of a phased array are then recorded on N lines at plane P_1. The 2-D transform of the light distribution transmitted through plane P_2 now has the compression and high signal-to-noise of matched filtering and coded waveforms. The coordinates of the output peak(s) of light are now proportional to the target's azimuth and range (for a phased array) or the target's Doppler and range (for a pulse burst radar) and thus constitutes the ambiguity function of the radar. Two examples are shown in Figure 7 for a target at azimuth angles of 5° and 30° and fine ranges of 45% and 55% of the range bin R_B.

6.4 Optical Correlation of Long Coded Waveforms [13]

The radar code is often quite long (e.g. 10^4 bits) and the linear resolution of an SLM cannot accommodate it. Another problem associated with such a code is the determination of where within the transmitted code a received code starts. For a long NM bit code, we devised an optical processor capable of solving both of the problems. The received signal is raster recorded on M lines with N points per line. A unique matched filter of only (2M-1)x(2N-1) bits was constructed. This is far less than the $(NM)^2$ bit size normally

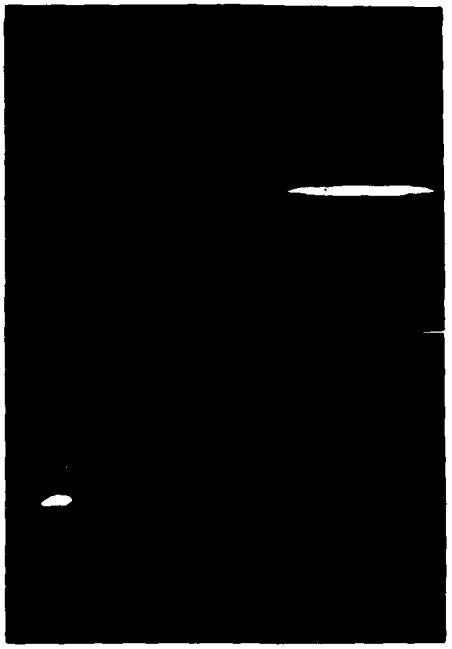

Fig. 7 Multi-channel 1-D optical processing for range/azimuth data (a) Target at 5° and 45% of the range bin; (b) Target at 30° and 55% of the range bin. [12]

required.) The system is most useful for pseudo-random codes. The output correlation plane pattern consists of a spot of light of full amplitude with its location proportional to the starting bit location of the received code within the full transmitted code.

7. OPTICAL IMAGE PROCESSING [7,14]

In this brief section, we have selected several image processing operations that can be performed directly on a stored image using photo DKDP and two optical pattern recognition or correlation examples. These latter examples were again performed on the hybrid processor of Figure 4 in real-time using the electron-beam addressed DKDP SLM in the input plane P_1.

7.1 Image Processing [14]

Three image processing operations performed in real time on an image stored on the photo-DKDP SLM without the need for external spatial filters etc. are described. In Figure 8a, we show an example of image addition. The two images were focussed onto the device using two separate exposures with the same polarity of control voltage across the DKDP. With this multiple image pattern stored on the photo-DKDP, the SLM was exposed to the second image with the polarity of the voltage across the photo-DKDP reversed. This results in the subtraction of two images as shown in Figure 8b. If the control voltage across the SLM is varied while an image (Figure 8c) is present, any image contours present in the image can be displayed shown in Figure 8d.

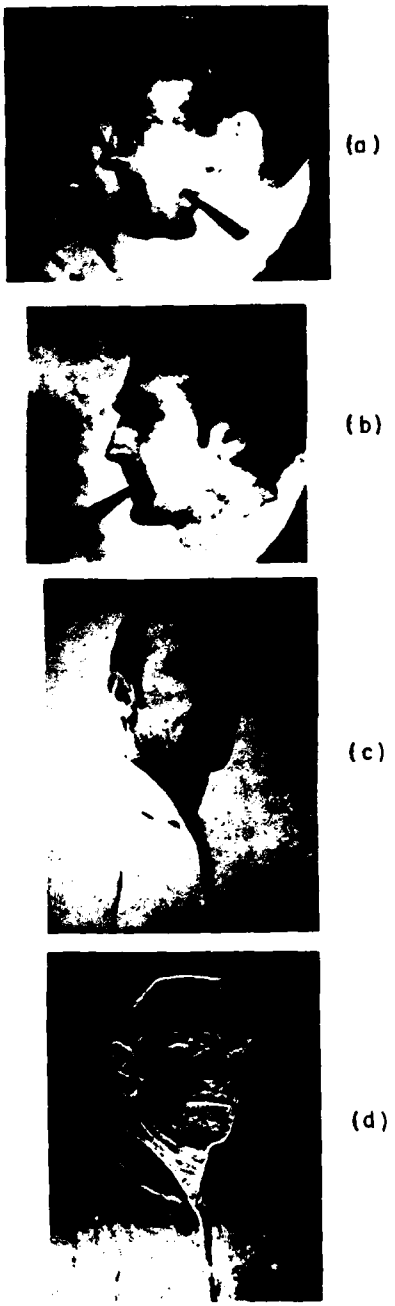

Fig. 8 Real-time image processing using photo-DKDP. (a) Image addition; (b) Image subtraction; (c) Input image; (d) Contour generation on the image in (c)[14]

7.2 Optical Pattern Recognition [7]

With an aerial image (Figure 9a) recorded on the electron-beam DKDP at plane P_1 of Figure 4 and a matched spatial filter of the desired reference function (Figure 9b) recorded at plane P_2, the output pattern at plane P_3 is the correlation of the input and reference functions. The amplitude of the output correlation peak is proportional to the agreement between the input and reference functions. The location of the output correlation peak is proportional to the location of the reference function in the input scene as shown in Figure 9c. The binary/digitized version of this pattern (Figure 9d) is easily determined by the digital system. The location of the correlation peak can be used as feedback control in a missile guidance application in which the input image originates from an on-board sensor and the reference image is one from a large stored data base.

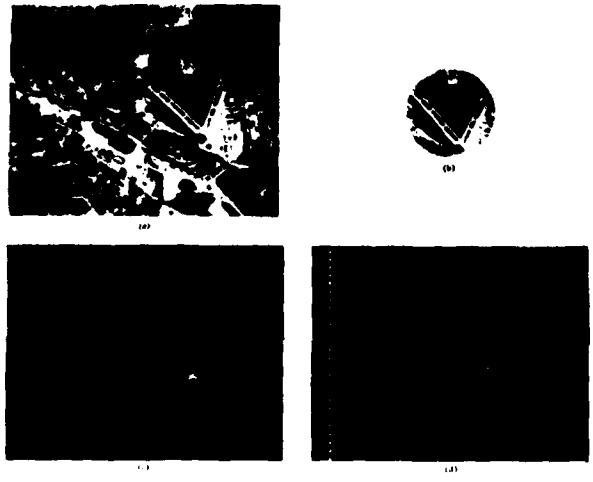

Fig. 9 Real-time optical pattern recognition of aerial imagery using electron-beam DKDP. (a) Input image; (b) Reference image; (c) Output correlation pattern; (d) Digitized version of (c) [7]

As noted earlier, the optical correlator of Figure 4 can be used with multiple occurences of a reference function. As an example of this, the input pattern of Figure 10a was recorded on the electron-beam DKDP at plane P_1 of Figure 4 and a matched spatial filter of the word "God" formed at plane P_2. The output correlation pattern at plane P_3 is shown in Figure 10b. After digital processing, the desired pattern of Figure 10c results in which the cross-correlation typical of text recognition have been removed and where the locations of each of the seven correlation peaks are proportional to the locations of the seven occurrences of the word "God" in the input image.

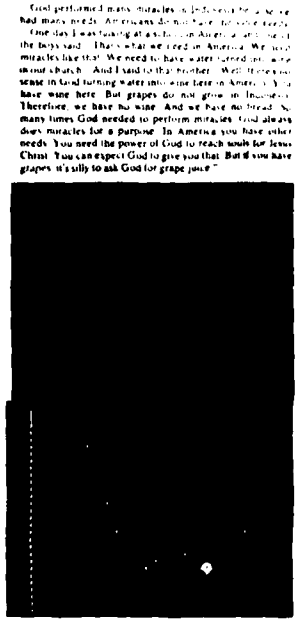

Fig. 10 Real-time optical pattern recognition of words using electron-beam DKDP. (a) Input pattern; (b) Optical correlation pattern of the word "God" and the image in (a); (c) Digitized version of (b). [7]

8. SPACE VARIANT OPTICAL PROCESSING [15,16]

To increase the flexibility of an optical processor and avoid several sources of correlation degradation such as scale and rotational changes between the input and reference functions, a space variant optical correlator has been suggested. A coordinate transformation $g_1(x) \rightarrow g_1(e^x)$ is applied to the input function (1-D functions are used for simplicity only) (here a simple log-scaling of the coordinates is used), and this new $g_1(e^x)$ function is recorded at P_1 of Figure 1. The Fourier transform of this function formed at P_2 is the Mellin transform $M_1(u)$ of $g_1(x)$. With M_1^* recorded at plane P_2, and a scaled version $g_2(ax)$ of g_1 recorded at P_1 as $g_2(e^{ax})$, the light distribution transmitted through P_2 is $M_1^* M_2$ where $M_2 = a^{ju} M_1 = M_1 \exp(jul na)$. Lens L_2 forms the Fourier transform of $M_1^* M_2$ and at plane P_3 we find

$$U_3(x) = g_1 \circledast g_2 = g_1 \circledast g_1 * \delta(x - \ln a) \quad (6)$$

From Eq. (6), we see the power of this system. The magnitude of the output correlation $g_1 \circledast g_2$ of two functions that differ in scale is identical to the auto-correlation $g_1 \circledast g_1$ of g_1 and thus there is no loss in signal-to-noise ratio and we have produced a scale invariant correlator. The delta function in Eq. (6) indicates that the location of the correlation peak is proportional

to the scale change between the input and reference functions.

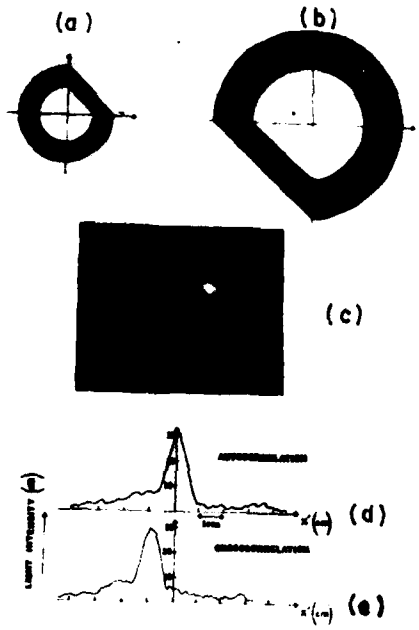

Fig. 11 Scale and rotation invariant correlation (a) Input; (b) Reference; (c) Output correlation; (d) Cross-section of auto-correlation; (e) Cross-section of cross-correlation [15]

A log-coordinate transform results in a scale invariant correlator as described above. To realize a rotational invariant correlator, a polar coordinate transform $f(x,y) \rightarrow f(r,\theta)$ is performed. With $\rho = e^r$ and the coordinate transformation $f(x,y) \rightarrow f(\rho,\theta)$, a scale and rotation invariant correlator results where the signal-to-noise of the output correlation is invariant to scale or rotation changes between the input and reference functions and where the coordinates of the output correlation peak are proportional respectively to the scale change and rotation differences between the input and reference. The correlation of the two inputs (Figures 11a and b) that differ in scale by 200% and are rotated by $\theta_o = 180°$ is shown in Figure 11c and the cross-sectional scans of the auto-correlation of one object and the cross-correlation of both objects in Figures 11d and 11e. As shown there is no signal-to-noise ratio loss and the displacement of the location of the correlation peak is proportional to the scale change between the objects.

The Mellin transform has immense practical use in Doppler signal processing. Since two signals that differ in Doppler have only a scale change between them, we can Mellin correlate these signals with no loss in signal-to-noise and from the location of the correlation peak determine the target's Doppler. An example of this using the correlator of Figure 2 with cylindrical/spherical lens pairs for L_1 and L_2 is shown in Figure 12. The same nine signals were recorded on one half of the input plane and nine different Doppler versions of the signal on the other half of the input plane (with a 100% Doppler difference across the signals). The output correlation plane pattern of Figure 12 shows nine correlation peaks of equal intensity, with the horizontal position of each spot proportional to the Doppler difference between the input signal on the respective line and the reference waveform.

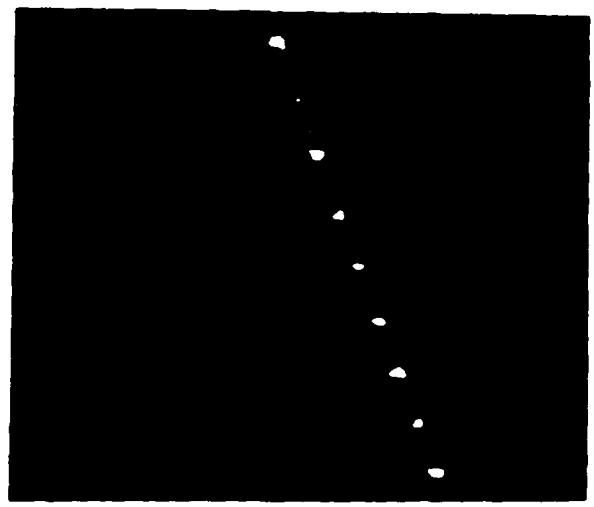

Fig. 12 Optical Doppler signal processing using Mellin transforms. [16]

9. SUMMARY AND CONCLUSION

From the selected examples above, the high space bandwidth, parallel processing, and signal and image processing applications of an optical processor are apparent. The hybrid and space variant processors described offer great promise for such systems and the development of novel data processing schemes.

ACKNOWLEDGEMENT

The author wishes to thank the members of his research group for their work included herein and the Office of Naval Research (Contracts NR048-600 and NR350-011), Air Force Office of Scientific Research (Grant AFOSR-75-2851), and the Ballistic Missile Defense Advanced Technology

Center (Contract DASG-60-77-C-0034) for their financial support of the research reported herein.

REFERENCES

1. A. Vander Lugt, Proc. IEEE, 62, 1300 (1974).

2. J. Goodman, Proc. IEEE, 65, (1977).

3. C. Thomas, Appl. Opt., 5, 1782 (1966).

4. D. Casasent and R. Kessler, Opt. Engr., Accepted (1977).

5. D. Casasent, Proc. IEEE, 65, 143 (1977).

6. D. Casasent, "Coherent Light Valves," in Appl. Opt. and Optical Engr., Ed. B.J. Thompson and R. Kingslake; Academic Press, NY (1978).

7. D. Casasent and W. Sterling, IEEE Trans. on Comput., C-24, 318 (1975).

8. D. Casasent, "Hybrid Processors," Chap. in Optical Data Processing, Ed. S. Lee, Springer-Verlag, Heidelberg (1978).

9. D. Casasent, "Optical Signal Processing," in Applications of Optical Data Processing, Ed. D. Casasent and H. J. Caulfield, Springer-Verlag, Heidelberg (1977).

10. D. Casasent and F. Casasayas, IEEE Trans. Aerosp. and Electr. Sys., AES-11, 65 (1975).

11. D. Casasent and F. Casasayas, Appl. Opt., 14, 1364 (1975).

12. D. Casasent and E. Klimas, IEEE Trans. Aerosp. and Electr. Sys., Submitted (1977).

13. D. Casasent and R. Kessler, Opt. Engr., 17, 242 (1976).

14. J. Donjon et al., IEEE Trans. Elec. Dev. ED-20, 1037 (1973).

15. D. Casasent and D. Psaltis, Proc. IEEE, 65, 77 (1977).

16. D. Casasent and D. Psaltis, Opt. Engr., 15, 258 (1976).

UNCLASSIFIED

SECURITY CLASSIFICATION OF THIS PAGE *(When Data Entered)*

(19) ~~REPORT DOCUMENTATION PAGE~~	READ INSTRUCTIONS BEFORE COMPLETING FORM
1. REPORT NUMBER (18) AFOSR-TR-78-0795	2. GOVT ACCESSION NO. 3. RECIPIENT'S CATALOG NUMBER (9)
4. TITLE *(and Subtitle)* (6) COHERENT OPTICAL DATA PROCESSING: A STATUS REPORT.	5. TYPE OF REPORT & PERIOD COVERED INTERIM rept.
	6. PERFORMING ORG. REPORT NUMBER (15) DAAG29-77-C-0034
7. AUTHOR(s) (10) David Casasent	8. CONTRACT OR GRANT NUMBER(s) AFOSR-75-2851 ✓
9. PERFORMING ORGANIZATION NAME AND ADDRESS Carnegie-Mellon University ✓ Pittsburgh, PA 15213	10. PROGRAM ELEMENT, PROJECT, TASK AREA & WORK UNIT NUMBERS 61102F (17) (16) 2305/B2
11. CONTROLLING OFFICE NAME AND ADDRESS AFOSR/NE Bldg 410 Bolling AFB DC 20332	12. REPORT DATE (11) 1977
	13. NUMBER OF PAGES 9
14. MONITORING AGENCY NAME & ADDRESS *(if different from Controlling Office)* (12) 10p.	15. SECURITY CLASS. *(of this report)* UNCLASSIFIED
	15a. DECLASSIFICATION/DOWNGRADING SCHEDULE

16. DISTRIBUTION STATEMENT *(of this Report)*

Approved for public release; Distribution unlimited

17. DISTRIBUTION STATEMENT *(of the abstract entered in Block 20, if different from Report)*

18. SUPPLEMENTARY NOTES

19. KEY WORDS *(Continue on reverse side if necessary and identify by block number)*

20. ABSTRACT *(Continue on reverse side if necessary and identify by block number)*

The operations possible in a coherent optical computer are briefly reviewed and several applications of this novel class of processor are included. Emphasis is given to signal processing operations and new space variant optical processor architectures.

DD FORM 1 JAN 73 1473 EDITION OF 1 NOV 65 IS OBSOLETE

403586

UNCLASSIFIED

SECURITY CLASSIFICATION OF THIS PAGE *(When Data Entered)*

Electronic
Aerospace systems

AIR FORCE OFFICE OF SCIENTIFIC RESEARCH (AFSC)
NOTICE OF TRANSMITTAL TO DDC
This technical report has been reviewed and is approved for publication. [illegible] AFR 190-12 (7b).
Distribution is unlimited.
A. D. BLOSE
Technical Information Officer